

Two Forms of Knowledge Representations in the Human Brain

Highlights

- Blind and sighted individuals perform object-color-knowledge tasks partially similarly
- Dorsal anterior temporal lobe represents object-color knowledge in both groups
- The visual cortex represents object-color knowledge in only the sighted group
- There are two types of knowledge representation for concepts with sensory referents

Authors

Xiaoying Wang, Weiwei Men,
Jiahong Gao, Alfonso Caramazza,
Yanchao Bi

Correspondence

ybi@bnu.edu.cn

In Brief

How is knowledge represented in the human brain? By comparing blind and sighted individuals' object-color-knowledge representation, Wang et al. provide evidence for two forms of knowledge representation for concepts with sensory referents, one derived from sensory experience and one from language and cognitive inference.



Article

Two Forms of Knowledge Representations in the Human Brain

Xiaoying Wang,^{1,2} Weiwei Men,^{3,4} Jiahong Gao,^{3,4,5} Alfonso Caramazza,^{6,7} and Yanchao Bi^{1,2,8,*}¹State Key Laboratory of Cognitive Neuroscience and Learning & IDG/McGovern Institute for Brain Research, Beijing Normal University, Beijing 100875, China²Beijing Key Laboratory of Brain Imaging and Connectomics, Beijing Normal University, Beijing 100875, China³Center for MRI Research, Academy for Advanced Interdisciplinary Studies, Peking University, Beijing 100871, China⁴Beijing City Key Lab for Medical Physics and Engineering, Institute of Heavy Ion Physics, School of Physics, Peking University, Beijing 100871, China⁵McGovern Institute for Brain Research, Peking University, Beijing 100871, China⁶Department of Psychology, Harvard University, Cambridge, MA 02138, USA⁷Center for Mind/Brain Sciences, University of Trento, 38068 Rovereto, Italy⁸Lead Contact*Correspondence: ybi@bnu.edu.cn<https://doi.org/10.1016/j.neuron.2020.04.010>

SUMMARY

Sensory experience shapes what and how knowledge is stored in the brain—our knowledge about the color of roses depends in part on the activity of color-responsive neurons based on experiences of seeing roses. We compared the brain basis of color knowledge in congenitally (or early) blind individuals, whose color knowledge can only be obtained through language descriptions and/or cognitive inference, to that of sighted individuals whose color-knowledge benefits from both sensory experience and language. We found that some regions support color knowledge only in the sighted, whereas a region in the left dorsal anterior temporal lobe supports object-color knowledge in both the blind and sighted groups, indicating the existence of a sensory-independent knowledge coding system in both groups. Thus, there are (at least) two forms of object knowledge representations in the human brain: sensory-derived and language- and cognition-derived knowledge, supported by different brain systems.

INTRODUCTION

Roses are red, violets are blue, so goes the poem. What is the neural code for such knowledge in the human brain? Although object knowledge can be acquired both through sensory experience (seeing red roses) and through language descriptions (e.g., being told by others that roses are “red”), one prominent theory assumes that such knowledge is stored in sensory association cortices, derived from sensory experiences (i.e., seeing the colors of roses) (Barsalou et al., 2003; Martin, 2016; Simmons et al., 2007). The alternative possibility is that even sensory-derived knowledge is also represented at an abstract conceptual level distinct from sensory representations (Leshinskaya and Caramazza, 2016; Mahon and Caramazza, 2008; Shallice, 1987, 1988; Wang et al., 2018; Xu et al., 2017).

Prior attempts to test the existence of and to characterize the neural representation of non-sensory-derived object knowledge include studies of congenitally, sensory-deprived populations (e.g., blind/deaf) as well as studies with sighted and blind individuals of abstract concepts such as “idea” that do not refer to specific sensory experiences. However, it has been argued that even such abstract concepts may still be

grounded in their associated sensory, emotional, and complex event experiences (Barsalou, 2008; Borghi and Binkofski, 2014; Kiefer and Pulvermüller, 2012; Kousta et al., 2011; Vigliocco et al., 2014). And, in the case of studies based on sensory deprivation, aspects of the knowledge not available from one sense could be obtained partially through other senses (Amedi et al., 2007; Ricciardi et al., 2014). For instance, object-shape knowledge can be obtained both by vision and by touch (Amedi et al., 2001; Lacey and Sathian, 2012, 2014; Peelen et al., 2014), object-motion information could be acquired by vision, touch, or sound (Noppeney et al., 2003). Given these considerations, the investigation of color knowledge in congenitally blind individuals, which is remarkably rich (Connolly et al., 2007; Landau, 1983; Landau and Gleitman, 1985; Marmor, 1978; Sayani et al., 2018; Shepard and Cooper, 1992), is especially appropriate for understanding sensory-independent representations. In these individuals, color knowledge can be obtained only through language descriptions (e.g., some roses are red; red is more similar to orange than to blue) and cognitive inference (Kim et al., 2019), providing a unique opportunity to test how and where such knowledge is represented in the brain. It also allows investigation of the relationship between



highly correlated (Figure 1A; Pearson $r = 0.88$, $n = 276$, $p < 3.91 \times 10^{-90}$). The same pattern of results was also obtained using the behavioral task requiring explicit color name generation for objects (Figure S1A). Multi-dimensional scaling (MDS) (Busing et al., 1997; Takane et al., 1977), using individual differences scaling solutions (INDSCAL), was carried out to visualize the object-color space in each group. This analysis revealed two highly similar two-dimensional object spaces for the EB and SC groups (Figure 1B; $r = 0.88$, $p < 5.85 \times 10^{-90}$). Within each object space, objects loosely clustered into those with red, ye

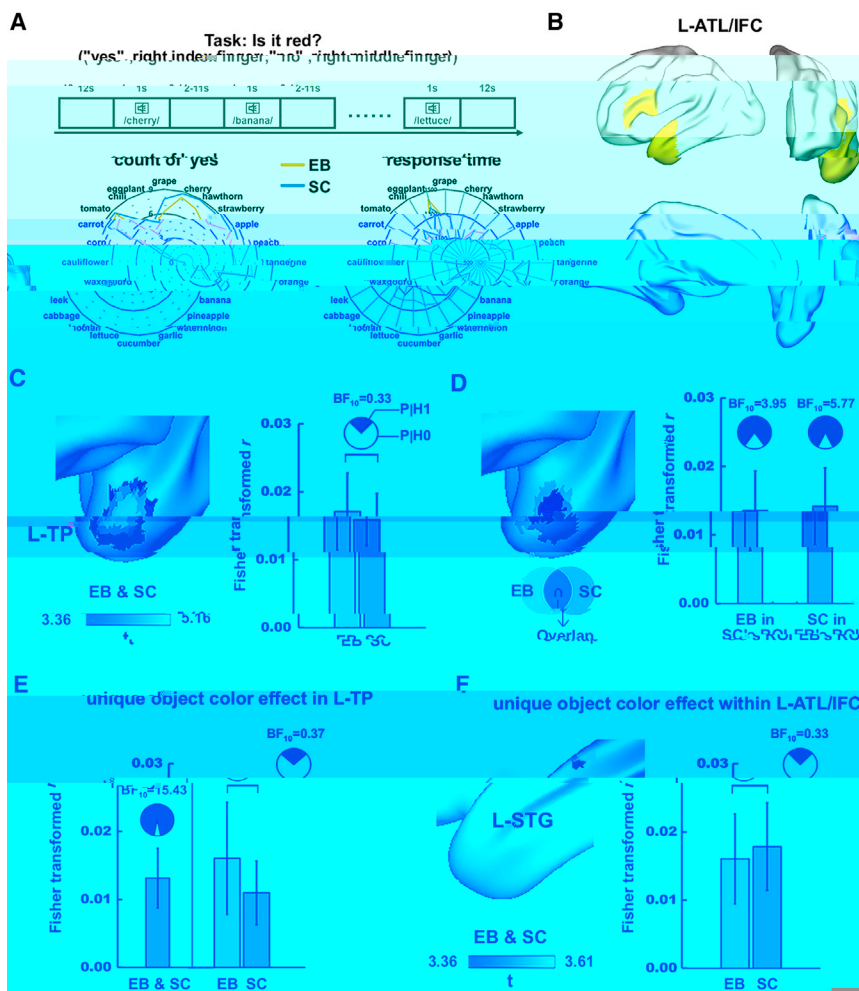


Figure 2. Object-Color Representation within the Left ATL/IFC

(A) Design and behavioral performances of the fMRI experiment.

(B) The anatomically defined left ATL/IFC (STAR Methods).

(C) Combination of object-color effect across the EB (n = 15) and the SC (n = 20) groups (voxel-level $p < 0.001$, one-tailed, cluster-level FWE-corrected $p < 0.05$). Color scale indicates corresponding t values. The bar plot shows the magnitude of the object-color effect (RSA-derived Fisher-transformed r values averaged across participants) in EB and SC groups in the left TP. Error bars indicate corresponding standard errors. The pie chart depicts the results of the Bayesian t tests: the odds of the data under H0 (white part) versus H1 (dark red part).

(D) The object-color effect in EB (voxel-level $p < 0.005$, one-tailed, cluster size = 46 voxels, uncorrected) and SC (voxel-level $p < 0.001$, one-tailed, cluster-level FWE-corrected $p < 0.05$), respectively, and their overlap (red patch). The bar plot shows the cross-group ROI analysis results: the object-color effect of SC group (blue bar) in EB's object-color cluster (red and yellow patches) and the object-color effect of EB group (yellow bars) in SC's significant object-color cluster (red and blue patches).

(E) The unique object-color effect in L-TP after controlling for other types of object knowledge (i.e., shape, taste, touch, and semantic relatedness). The orange bar indicates the combined unique object-color effect in L-TP. The yellow and the blue bars show EB and SC's unique object-color effect, respectively.

(F) Combination of unique object-color effect across EB and SC groups within the L-ATL/IFC mask (voxel-level $p < 0.001$, one-tailed, cluster size = 13 voxels, uncorrected). The bar plot is similar to the one in (C). Color scale indicates corresponding t values.

across voxels for each participant, and compared between groups. A two-sample t test using the bootstrap resampling method (n = 10,000) did not reveal a significant between-group difference (mean difference \pm SE = 0.001 \pm 0.007, two-tailed $p = 0.857$). A Bayesian independent samples t test (Wagenmakers et al., 2018a, 2018b) was further conducted to measure the strength of evidence for H0 (EB = SC) and H1 (EB \neq SC). The result revealed moderate evidence in favor of H0 ($BF_{10} = 0.33$), confirming that both groups exhibited comparable object-color representations in the L-TP.

RSA searchlight analyses of the object-color-knowledge representation, separately in each group, converged on finding this dorsal ATL cluster (Figure 2D; Table 1): a dorsal TP cluster exhibited significant object-color-knowledge representation in the SC group (Figure 2D, blue and red; voxel-level $p < 0.001$, cluster-level FWE-corrected $p < 0.05$). RSA-based ROI analysis in this cluster revealed a significant object-color effect also in the EB group (Figure 2D, bar plot, yellow bar; bootstrap-resampling one-sample t test: mean \pm SE = 0.013 \pm 0.006, one-tailed $p = 0.015$; Bayesian one-sample t test: $BF_{10} = 3.95$, moderate

evidence in favor of H1: group mean >0). For the EB group, the object-color effect was weaker, without any results surviving the conventional threshold, which might be due to smaller sample size, but still showed the strongest trend in the left dorsal TP cluster (Figure 2D, yellow and red; uncorrected voxel-level $p < 0.005$, one-tailed, 47 voxels). RSA-based ROI analysis in the EB's L-TP cluster also revealed significant object-color effect in the SC group (Figure 2D, bar plot, blue bar; bootstrap-resampling one-sample t test: mean \pm SE = 0.014 \pm 0.005, one-tailed $p = 0.010$; Bayesian one-sample t test: $BF_{10} = 5.77$, moderate evidence in favor of H1: group mean >0). A between-group comparison of the RSA searchlight results did not reveal any cluster showing a difference between EB and SC groups even under an extremely low threshold (voxel-level $p < 0.01$, cluster size >10 voxels).

The object-color-knowledge representation effects in the left ATL are not attributable to other object features that correlated with object-color knowledge. We first conducted a follow-up partial correlation analysis (Figure 2E) between the neural RSM and the object-color behavioral RSM while controlling

for the RSMs of other types of object knowledge (i.e., shape, taste, touch, and semantic relatedness). Partial correlations were computed for each sphere (6 mm radius) centered at each voxel in the L-TP, and the resulting r values (Fisher-transformed) were averaged across voxels for each participant. One-sample t test using the bootstrap resampling method ($n = 10,000$) revealed a positive partial correlation significantly higher than zero across all participants in the L-TP (Figure 2E, orange bar; mean \pm SE = 0.013 ± 0.004 , one-tailed $p = 0.002$). A Bayesian one-sample t test also revealed strong evidence in favor of positive unique object-color representation ($BF_{10} = 15.43$) in the L-TP. In addition, independent-samples t tests did not reveal significant between-group difference of the partial correlations in L-TP (Figure 2E, yellow and blue bars; bootstrap resampling result: mean \pm SE = 0.005 ± 0.009 , two-tailed $p = 0.595$; Bayesian method result: $BF_{10} = 0.37$, anecdotal evidence in support of H_0 : EB = SC). Note that replacing semantic relatedness rating with taxonomy categories (fruit versus vegetable) yielded almost identical results (Figure S3). These results confirm that the object-color-knowledge representation we observed in the L-TP is not driven by other types of object knowledge. We also searched for regions showing unique object-color representation within the left ATL/IFC mask to check for potential effects beyond the L-TP ROI. The analysis revealed a more posterior and dorsal cluster in the left anterior superior temporal gyrus (STG) showing a trend of unique object-color effect when combining the two groups (Figure 2F; Table 1; voxel-level $p <$

0.001 , one-tailed, 13 voxels, uncorrected). ROI analysis on this L-STG cluster did not reveal a significant difference between EB and SC groups, suggesting that both groups tend to show comparable unique object-color representation in this region (Figure 2F, bar plot; bootstrap resampling: mean \pm SE = -0.002 ± 0.009 , two-tailed $p = 0.850$; Bayesian: $BF_{10} = 0.37$, anecdotal evidence in support of H_0 : EB = SC).

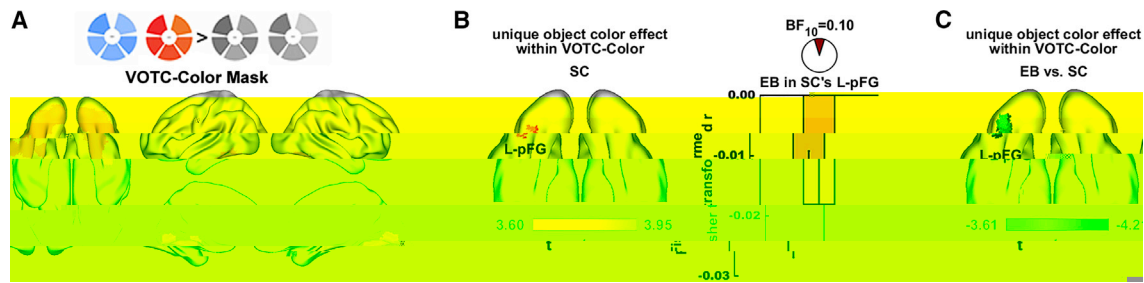


Figure 3. Object-Color Representation within the VOTC Color

(A) Color-sensitive VOTC regions defined from the color perceptual localizer (see STAR Methods).

(B) The left pFG showing significant unique object-color effect in the SC group (voxel-level $p < 0.001$, one-tailed, cluster-level FWE-corrected $p < 0.05$). The bar plot shows the EB's unique object-color effect in the left pFG. The error bar indicates the corresponding standard error. The pie chart depicts the result of the Bayesian t-tests: the odds of the data under H_0 (white part) vs. H_1 (dark red part).

(C) Between-group comparison of the unique object-color effect within VOTC-color. Color scales indicate corresponding t values. Cold color indicates stronger effects in SC relative to in EB.

reported that color-perception and object-color-knowledge retrieval activated overlapping or adjoining regions in VOTC and suggested that these regions play a role in grounding conceptual knowledge through perceptual simulation (Martin, 2016; Simmons et al., 2007).

In this VOTC-color mask, when analyzing the two groups combined, no significant effect was obtained even at an ultra-low threshold (voxel-level $p < 0.01$, one-tailed, cluster size >10 voxels). RSA searchlight analyses in each group separately revealed that the SC group showed significant unique object-color representation in the left posterior fusiform gyrus (pFG) at the conventional threshold (voxel-level $p < 0.001$, one-tailed, cluster-level FWE-corrected $p < 0.05$; Figure 3B; Table 2). The EB group showed no effect of unique object-color-knowledge representation in either RSA-based ROI analysis in this cluster (Figure 3B, bar plot; bootstrap resampling one sample t test: mean \pm SE = -0.018 ± 0.009 , one-tailed $p = 0.968$; Bayesian one sample t test, H_1 : group mean > 0 , $BF_{10} = 0.10$, strong evidence in favor of H_0) or in the RSA searchlight mapping within the VOTC-color mask (no cluster found even at an ultra-low threshold of uncorrected $p < 0.01$, one-tailed, cluster size >10 voxels). A between-group comparison of the RSA searchlight results revealed significantly stronger unique object-color representation in the SC relative to the EB group in the left pFG (Figure 3C; Table 2; voxel-level $p < 0.001$, two-tailed, cluster-level FWE-corrected $p < 0.05$; neural RSMs shown in Figure S5). Similar patterns of RSA results were observed for object-color-knowledge effect without controlling for other object features (Figure S6; Table 2).

Validation of the Neural Substrates for Object-Color-Knowledge Representation in Blind and Sighted Participants

The following set of validation analyses were conducted: (1) RSA searchlight mapping further controlling for response-time and button-press patterns during fMRI scanning (Figure S7); (2) RSA searchlight mapping using object-color RSMs derived from other color-knowledge behavioral tests (i.e., verbal generation of object-color names; color word similarity rating) (Figure S8); (3) analysis addressing individual variability (Figure S9); and (4) laterality analysis of object-color

representation in ATL and VOTC. The main pattern of results remained across these validation analyses, after controlling for peripheral response variables, using the new behavioral measure for object-color-knowledge space construction, or removing outliers. By computing the laterality index of object-color representation in the bilateral ATL and VOTC, we observed left-laterality in ATL in both EB (moderate to strong) and SC (trend to moderate) group, and bilaterality to moderate left-laterality in SC in VOTC. Detailed results are presented in the Data S1 and supplemental figures (Figures S7–S9).

Whole-Brain Searchlight Results

The object-color-knowledge representation results in whole-brain analyses converged well with the results within the two pre-defined masks reported above. Combining the two groups, RSA searchlight mapping in the whole brain revealed that clusters in the left dorsal TP and the anterior STG showed significant object-color-knowledge representation (voxel $p < 0.001$, one-tailed, cluster-level FWE-corrected $p < 0.05$; Figures 4A and 4C; Table S3). RSA-based ROI analyses in these clusters did not reveal any significant between-group difference (Figures 4A and 4C, bar plots; Table S3). Contrasting the two groups revealed stronger effects of object-color-knowledge representation in the SC relative to the EB group at a lenient threshold in the posterior VOTC regions, and small clusters scattered in the left temporoparietal, the left anterior inferior temporal and the ventral medial prefrontal cortex (Figures 4B and 4D; Table S3; voxel-level $p < 0.001$, two-tailed, cluster size >10 voxels, uncorrected).

Different Functional Networks for Object-Color Knowledge in Blind and Sighted Individuals

The intrinsic resting-state functional connectivity (rsFC) profile of the object-color-knowledge representation nodes obtained above—the vision-independent left anterior dorsal ATL (L-adATL; combining L-TP and L-STG in Figures 4A and 4C) and the vision-dependent posterior VOTC perception node (left pFG in Figure 3C)—showed interesting differences between the EB and the SC participants (Figure 5A; Table 3; ROI-wised

connectivity, Bonferroni corrected $p < 0.05$, number of multiple comparisons = 5). While for the EB group there was no significant connection between vision-independentno significant connection

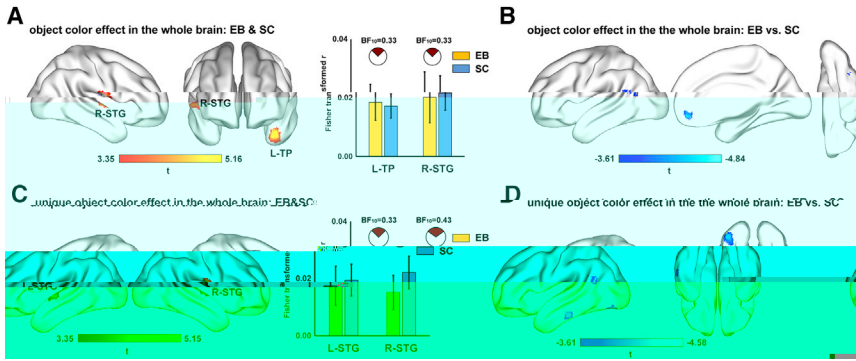


Figure 4. Object-Color Representation in the Whole Brain

(A) Combination of object-color effects across the EB and the SC groups (voxel-level $p < 0.001$, one-tailed, cluster-level FWE-corrected $p < 0.05$). The bar plot shows the extent of object-color effect in the EB and the SC groups in the identified clusters. The pie charts depict the odds of the data under H0 (white part) versus H1 (dark red part). Error bars indicate standard errors.

(B) Between-group comparison of object-color effect (voxel-level $p < 0.001$, two-tailed, cluster size >10 voxels, uncorrected).

(C) Combination of unique object-color effects across the EB and the SC groups. The effects explained by object shape, taste, touch, and

semantic relatedness were removed using partial correlation (voxel-level $p < 0.001$, one-tailed, cluster-level FWE-corrected $p < 0.05$).

(D) Between-group comparison of unique object-color effects (voxel-level $p < 0.001$, two-tailed, cluster size >10 voxels, uncorrected). Color scales indicate t values. Cold color indicates weaker effect in EB relative to in SC. Error bars indicate standard errors.

2016) in sighted people. Our results that color knowledge was not found to be encoded in the vicinity of these regions in the case of visual deprivation is in favor of the view that these areas encode visual-experience-derived representations (see also Bottini et al., 2020 for convergent evidence using an adaptation approach).

Critically, the only cluster showing object-color-knowledge representation in the early blind—dorsal ATL—also showed comparable effects in the sighted. Given that in the early blind color knowledge can be obtained only through language and cognitive inference, this overlap with the sighted indicates that even when color knowledge can be obtained through vision, the language/cognition-derived knowledge representation is also present. In other words, while in sighted people object-color knowledge can be acquired through vision, non-sensory-derived representations of color knowledge are present in dorsal ATL just as in blind people. This non-sensory, language/cognition-derived knowledge representation cluster aligns well with the ATL regions showing stronger activation for abstract relative to concrete words (e.g., justice > cup) (Binder et al., 2009; Wang et al., 2010, 2019), and words referring to objects that are not perceptible relative to those that are (e.g., rainbow versus rain for congenitally blind, Striem-Amit et al., 2018), and regions showing adaptation effects for perceptual similarity judgment of color words in early blind (Bottini et al., 2020). These findings

led to the hypothesis that abstract concepts rely more on dorsal ATL due to their heavier reliance on the language system, while concrete concepts rely more on sensory-motor modalities (Dove, 2009; Wang et al., 2010, 2019). However, we showed that, even for knowledge that is “concrete” and “perceptible” such as object color, it too is represented in a region that is more closely related to the language system. Thus, it is not whether the knowledge has a perceptible/concrete referent or not, but the level of abstractness of the knowledge coding (i.e., cognitively derived versus sensory derived) that determines whether it is represented in dorsal ATL. Corroborating these findings, the rsFC results showed that the dorsal ATL is strongly connected with the regions implicated in language processing (Figure 5A), which require a high degree of generality and abstractness. This may also explain the effects of bilateral STG, a part of the language system (Fedorenko et al., 2010), in the whole-brain search light analysis (Figure 4).

There are a few empirical points to be considered in this context. First, the univariate contrasts in previous studies showed greater advantage for abstract over concrete concepts in dorsal ATL (Binder et al., 2009; Wang et al., 2010, 2019). If knowledge referring to perceptible properties and entities is also represented in this region, in a language- (and cognitively) derived format, then why the abstract advantage? We speculate that for the perceptible and/or concrete case, there is a network

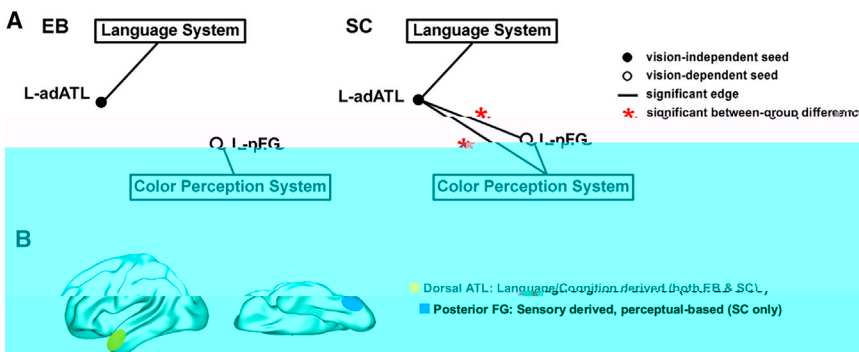


Figure 5. Different Functional Connectivity Patterns in EB and SC and a Schematic View of the Dual Forms of Knowledge Representation in the Human Brain

(A) Different rsFC networks in EB and SC group. Black disks indicate vision-independent object-color node and circles indicate vision-dependent object-color nodes. Solid lines indicate significant positive connections (Bonferroni corrected, number of comparisons = 5), respectively. Red asterisks indicate stronger connection strengths in SC relative to in EB group (Bonferroni corrected, $P < 0.05$).

(B) A schematic view of coexisting language/cognition-derived and sensory-derived knowledge representations in the human brain.

with multiple additional regions that represent such knowledge (see Figure 5B), and thus the activation strength may be diluted across the network. Second, neuropsychological studies have reported patients with specific object-color-knowledge impairment, who have lesions in occipitotemporal cortex extending to the ventral medial temporal pole regions (Miceli et al., 2001; Stassenko et al., 2014) but sparing the dorsal anterior regions of color-knowledge representation reported here. If the dorsal ATL color patch is sufficient to support normal color-knowledge behavior in the blind group as shown here, why do the color agnosia patients with spared dorsal ATL have color-knowledge deficits? The seemingly contrasting results could reflect effects of the network structure of these nodes in the sighted brain (Figure 5). Given the intrinsic functional connectivity between the ventral posterior sensory-derived nodes and the dorsal anterior language/cognition-derived nodes in the sighted brain, lesions to one may affect the functionality of the others, and/or the integrity of the whole network might be necessary for normal behavior. Indeed, a recent study (Siuda-Krzywicka et al., 2019) reported a patient with a lesion that disconnected color-biased visual regions from the dorsal and lateral part of the left ATL, who showed color-naming deficits despite intact color categorical perception. This profile is in line with our speculation that the disruption of part of the functional networks (any node and/or connection) may affect the functionality of other components with consequences on the corresponding behavior.

To conclude, we have provided clear, positive evidence for an independent language/cognition-derived neural representation of object knowledge in addition to sensory-derived representations. This multiple-type representation neural framework for object knowledge opens up new lines of research questions in the study of the biological basis of memory, about the nature of each of these forms, about the interaction between these forms, and about the potential similarity and differences about information stores in the human versus non-human brains.

STAR★METHODS

Detailed methods are provided in the online version of this paper and include the following:

- KEY RESOURCES TABLE
- RESOURCE AVAILABILITY
 - Lead Contact

- Materials Availability
- Data and Code Availability
- EXPERIMENTAL MODEL AND SUBJECT DETAILS
- METHOD DETAILS
 - Stimuli
 - Behavioral tests
 - Procedures for task-fMRI experiment
 - Image acquisition
- QUANTIFICATION AND STATISTICAL ANALYSIS
 - Data preprocessing
 - Data analysis

SUPPLEMENTAL INFORMATION

Supplemental Information can be found online at <https://doi.org/10.1016/j.neuron.2020.04.010>.

ACKNOWLEDGMENTS

We thank Dr. Yangwen Xu for helpful discussions regarding experimental design and help in data collection. We thank all the blind subjects who participated in our experiment. This work was supported by the National Natural Science Foundation of China (31925020 and 31671128 to Y.B.; 31500882 to X.W.), Changjiang Scholar Professorship Award (T2016031 to Y.B.), the Fundamental Research Funds for the Central Universities (2017EYT35 to Y.B.), the 111 Project (BP0719032 to Y.B.), and the Interdisciplinary Research Funds of Beijing Normal University (to Y.B.). We also thank the National Center

- Amedi, A., Stern, W.M., Camprodon, J.A., Bermpohl, F., Merabet, L., Rotman, S., Hemond, C., Meijer, P., and Pascual-Leone, A. (2007). Shape conveyed by visual-to-auditory sensory substitution activates the lateral occipital complex. *Nat. Neurosci.* 10, 687–689.
- Ashburner, J. (2007). A fast diffeomorphic image registration algorithm. *Neuroimage* 38, 95–113.
- Bannert, M.M., and Bartels, A. (2013). Decoding the yellow of a gray banana. *Curr. Biol.* 23, 2268–2272.
- Bannert, M.M., and Bartels, A. (2018). Human V4 Activity Patterns Predict Behavioral Performance in Imagery of Object Color. *J. Neurosci.* 38, 3657–3668.
- Barsalou, L.W. (2008). Grounded cognition. *Annu. Rev. Psychol.* 59, 617–645.
- Barsalou, L.W., Kyle Simmons, W., Barbey, A.K., and Wilson, C.D. (2003). Grounding conceptual knowledge in modality-specific systems. *Trends Cogn. Sci.* 7, 84–91.
- Beauchamp, M.S., Haxby, J.V., Jennings, J.E., and DeYoe, E.A. (1999). An fMRI version of the Farnsworth-Munsell 100-Hue test reveals multiple color-selective areas in human ventral occipitotemporal cortex. *Cereb. Cortex* 9, 257–263.
- Binder, J.R., Desai, R.H., Graves, W.W., and Conant, L.L. (2009). Where is the semantic system? A critical review and meta-analysis of 120 functional neuroimaging studies. *Cereb. Cortex* 19, 2767–2796.
- Binney, R.J., Hoffman, P., and Lambon Ralph, M.A. (2016). Mapping the Multiple Graded Contributions of the Anterior Temporal Lobe Representational Hub to Abstract and Social Concepts: Evidence from Distortion-corrected fMRI. *Cereb. Cortex* 26, 4227–4241.
- Borghi, A.M., and Binkofski, F. (2014). Words as Social Tools: An Embodied View on Abstract Concepts (Springer).
- Bottini, R., Ferraro, S., Nigri, A., Cuccarini, V., Bruzzone, M.G., and Collignon, O. (2020). Brain Regions Involved in Conceptual Retrieval in Sighted and Blind People. *J. Cogn. Neurosci.* Published online February 4, 2020. https://doi.org/10.1162/jocn_a_01538.
- Busing, F., Commandeur, J.J.F., and Heiser, W.J. (1997). PROXSCAL: A Multidimensional Scaling Program for Individual Differences Scaling with Constraints (Softstat).
- Connolly, A.C., Gleitman, L.R., and Thompson-Schill, S.L. (2007). Effect of congenital blindness on the semantic representation of some everyday concepts. *Proc. Natl. Acad. Sci. USA* 104, 8241–8246.
- Davies, P.M., and Coxon, A.P.M. (1982). Key Texts in Multidimensional Scaling (Heinemann Educational).
- Dove, G. (2009). Beyond perceptual symbols: a call for representational pluralism. *Cognition* 110, 412–431.
- Efron, B., and Tibshirani, R.J. (1993). An Introduction to the Bootstrap (CRC Press).
- Fedorenko, E., Hsieh, P.-J., Nieto-Castañón, A., Whitfield-Gabrieli, S., and Kanwisher, N. (2010). New method for fMRI investigations of language: defining ROIs functionally in individual subjects. *J. Neurophysiol.* 104, 1177–1194.
- Goldberg, R.F., Perfetti, C.A., and Schneider, W. (2006). Perceptual knowledge retrieval activates sensory brain regions. *J. Neurosci.* 26, 4917–4921.
- Hoffman, P., Binney, R.J., and Lambon Ralph, M.A. (2015). Differing contributions of inferior prefrontal and anterior temporal cortex to concrete and abstract conceptual knowledge. *Cortex* 63, 250–266.
- Hsu, N.S., Kraemer, D.J.M., Oliver, R.T., Schlichting, M.L., and Thompson-Schill, S.L. (2011). Color, context, and cognitive style: variations in color knowledge retrieval as a function of task and subject variables. *J. Cogn. Neurosci.* 23, 2544–2557.
- Kiefer, M., and Pulvermüller, F. (2012). Conceptual representations in mind and brain: theoretical developments, current evidence and future directions. *Cortex* 48, 805–825.
- Kim, J.S., Elli, G.V., and Bedny, M. (2019). Knowledge of animal appearance among sighted and blind adults. *Proc. Natl. Acad. Sci. USA* 116, 11213–11222.
- Kousta, S.-T., Vigliocco, G., Vinson, D.P., Andrews, M., and Del Campo, E. (2011). The representation of abstract words: why emotion matters. *J. Exp. Psychol. Gen.* 140, 14–34.
- Kriegeskorte, N., Goebel, R., and Bandettini, P. (2006). Information-based functional brain mapping. *Proc. Natl. Acad. Sci. USA* 103, 3863–3868.
- Kriegeskorte, N., Mur, M., and Bandettini, P. (2008). Representational similarity analysis - connecting the branches of systems neuroscience. *Front. Syst. Neurosci.* 2, 4.
- Lacey, S., and Sathian, K. (2012). Representation of Object Form in Vision and Touch (CRC Press/Taylor & Francis).
- Lacey, S., and Sathian, K. (2014). Visuo-haptic multisensory object recognition, categorization, and representation. *Front. Psychol.* 5, 730.
- Lafer-Sousa, R., Conway, B.R., and Kanwisher, N.G. (2016). Color-Biased Regions of the Ventral Visual Pathway Lie between Face- and Place-Selective Regions in Humans, as in Macaques. *J. Neurosci.* 36, 1682–1697.
- Lambon Ralph, M.A., Jefferies, E., Patterson, K., and Rogers, T.T. (2017). The neural and computational bases of semantic cognition. *Nat. Rev. Neurosci.* 18, 42–55.
- Landau, B. (1983). Blind children's language is not meaningless. In *Language Acquisition in the Blind Child: Normal and Deficient*, D. Ling, ed. (College-Hill Press), pp. 62–76.
- Landau, B., and Gleitman, L.R. (1985). *Language and Experience: Evidence from the Blind Child* (Harvard University Press).
- Leshinskaya, A., and Caramazza, A. (2016). For a cognitive neuroscience of concepts: Moving beyond the grounding issue. *Psychon. Bull. Rev.* 23, 991–1001.
- Mahon, B.Z., and Caramazza, A. (2008). A critical look at the embodied cognition hypothesis and a new proposal for grounding conceptual content. *J. Physiol. Paris* 102, 59–70.
- Marmor, G.S. (1978). Age at onset of blindness and the development of the semantics of color names. *J. Exp. Child Psychol.* 25, 267–278.
- Martin, A. (2016). GRAPES-Grounding representations in action, perception, and emotion systems: How object properties and categories are represented in the human brain. *Psychon. Bull. Rev.* 23, 979–990.
- Miceli, G., Fouch, E., Capasso, R., Shelton, J.R., Tomaiuolo, F., and Caramazza, A. (2001). The dissociation of color from form and function knowledge. *Nat. Neurosci.* 4, 662–667.
- Misaki, M., Kim, Y., Bandettini, P.A., and Kriegeskorte, N. (2010). Comparison of multivariate classifiers and response normalizations for pattern-information fMRI. *Neuroimage* 53, 103–118.
- Noppeney, U., and Price, C.J. (2004). Retrieval of abstract semantics. *Neuroimage* 22, 164–170.
- Noppeney, U., Friston, K.J., and Price, C.J. (2003). Effects of visual deprivation on the organization of the semantic system. *Brain* 126, 1620–1627.
- Peelen, M.V., He, C., Han, Z., Caramazza, A., and Bi, Y. (2014). Nonvisual and visual object shape representations in occipitotemporal cortex: evidence from congenitally blind and sighted adults. *J. Neurosci.* 34, 163–170.
- Ricciardi, E., Bonino, D., Pellegrini, S., and Pietrini, P. (2014). Mind the blind brain to understand the sighted one! Is there a supramodal cortical functional architecture? *Neurosci. Biobehav. Rev.* 41, 64–77.
- Rouder, J.N., Morey, R.D., Speckman, P.L., and Province, J.M. (2012). Default Bayes factors for ANOVA designs. *J. Math. Psychol.* 56, 356–374.
- Sayani, A., Corballis, M.C., and Corballis, P.M. (2018). Colour envisioned: concepts of colour in the blind and sighted. *Vis. Cogn.* 26, 382–392.
- Schneider, W., Eschman, A., and Zuccolotto, A. (2002). E-Prime reference guide. *Psychol. Softw. Tools* 3, 1.
- Shallice, T. (1987). Impairments of semantic processing: Multiple dissociations. In *The Cognitive Neuropsychology of Language*, M. Coltheart, G. Sartori, and R. Job, eds. (Lawrence Erlbaum Associates Ltd.), pp. 111–127.
- Shallice, T. (1988). Specialisation within the semantic system. *Cogn. Neuropsychol.* 5, 133–142.

Shepard, R.N., and Cooper, L. (1992). Representation of Colors in the Blind, Color-Blind and Normally Sighted. *Psychol. Sci.* 3, 97–104.

Simmons, W.K., Ramjee, V., Beauchamp, M.S., McRae, K., Martin, A., and Barsalou, L.W. (2007). A common neural substrate for perceiving and knowing about color. *Neuropsychologia* 45, 2802–2810.

Siuda-Krzywicka, K., Witzel, C., Chabani, E., Taga, M., Coste, C., Cools, N., Ferrieux, S., Cohen, L., Seidel Malkinson, T., and Bartolomeo, P. (2019). Color Categorization Independent of Color Naming. *Cell Rep.* 28, 2471–2479.

Song, X.-W., Dong, Z.-Y., Long, X.-Y., Li, S.-F., Zuo, X.-N., Zhu, C.-Z., He, Y., Yan, C.-G., and Zang, Y.-F. (2011). REST: a toolkit for resting-state functional magnetic resonance imaging data processing. *PLoS ONE* 6, e25031.

Stasenko, A., Garcea, F.E., Dombrov, M., and Mahon, B.Z. (2014). When con-

STAR★METHODS

KEY RESOURCES TABLE

REAGENT or RESOURCE	SOURCE	IDENTIFIER
Deposited Data		
Behavior&Brain Data	This paper	https://osf.io/2ehu3/?view_only=5708ee4f21994105a47582652d6e3282
Software and Algorithms		
MATLAB	Mathworks	RRID: SCR_001622; https://www.mathworks.com/
SPM	FIL	RRID:SCR_007037; https://www.fil.ion.ucl.ac.uk/spm/
Statistical non-Parametric Mapping	University of Michigan; Michigan; USA, University of Warwick; Coventry; United Kingdom	RRID:SCR_002092; https://warwick.ac.uk/snpm
DPABI	Yan et al., 2016	RRID:SCR_010501; http://rfmri.org/dpabi
REST: a toolkit for resting-state fMRI	Song et al., 2011	RRID:SCR_009641; http://www.restfmri.net
JASP	The JASP Team	RRID:SCR_015823; https://jasp-stats.org/
E-prime	Psychology Software Tools	RRID:SCR_009567; https://www.pstnet.com/eprime.cfm
SPSS	IBM	RRID:SCR_002865; http://www.ibm.com/www-01.ibm.com/software/uk/analytics/spss/
BrainNet Viewer	Xia et al., 2013	RRID:SCR_009446; https://www.nitrc.org/projects/bnv/

RESOURCE AVAILABILITY

Lead Contact

Further information and requests for resources should be directed to and will be fulfilled by the Lead Contact, Yanchao Bi (ybi@bnu.edu.cn).

Materials Availability

This study did not generate new unique reagents.

Data and Code Availability

The data that support the findings of this study are available at https://osf.io/2ehu3/?view_only=5708ee4f21994105a47582652d6e3282.

EXPERIMENTAL MODEL AND SUBJECT DETAILS

Task-induced and resting-state fMRI data as well as behavioral data were collected from congenitally (or early) blind individuals and sighted controls.

15 congenitally (or early) blind (EB, 3 females) and 20 sighted controls (SC, 6 females) participated in the object color verification fMRI experiment. Ages and years of formal education were matched between EB (age: mean \pm SD = 44 \pm 12, range = 24 - 65; year of education: mean \pm SD = 11 \pm 3, range = 0 - 15) and SC (age: mean \pm SD = 43 \pm 11, range = 23 - 62, $|t_{(33)}| < 0.31$; years of education: mean \pm SD = 12 \pm 4, range = 9 - 19, $|t_{(33)}| < 1.24$).

13 EB (3 females) and 14 SC (4 females) with matched ages (EB: mean \pm SD = 44 \pm 11, range = 22 - 63; SC: mean \pm SD = 40 \pm 12, range = 22 - 60; $t_{(25)} < 1$) and years of formal education (EB: mean \pm SD = 12 \pm 2, range = 9 - 15; SC: mean \pm SD = 12 \pm 3, range = 9 - 18; $t_{(25)} < 1$) participated in the behavioral tests. All of the EB and 7 of the SC participants also took part in the object color verification fMRI experiment. The 14 SC participants also underwent a color perceptual localizer scanning.

14 EB (4 females) and 23 SC (8 females) matched in age (EB: mean \pm SD = 44 \pm 11, range = 22 - 63; SC: mean \pm SD = 41 \pm 14, range = 22 - 66; $t_{(34)} < 1$) and years of formal education (EB: mean \pm SD = 12 \pm 2, range = 9 - 15; SC: mean \pm SD = 12 \pm 4, range = 6 - 18; $t_{(34)} < 1$) participated in an 8-minute-long (240 volumes) resting-state fMRI scan. Thirteen of the EB and 7 of the SC participants also took part in the object color verification fMRI experiment. For these participants, the resting-state scan was performed about 2 years before the object color verification fMRI experiment.

All blind participants reported that they had been blind since birth. Because medical records of onset of blindness were not available for most participants, it cannot be ruled out that some of the participants may have had vision very early in life. None of the participants remembered to have ever been able to visually recognize shapes. Five blind participants reported to have had faint light perception in the past. Three blind participants had faint light perception at the time of testing. Detailed diagnoses for all blind participants are listed in [Table S1](#).

All participants were native Mandarin Chinese speakers. None had a history of psychiatric or neurological disorders or suffered from head injuries. All sighted participants had normal or corrected-to-normal vision and intact color perception. All participants provided informed consent and received monetary compensation for their participation. The study was approved by the Human Subject Review Committee at Peking University, China, in accordance with the Declaration of Helsinki.

METHOD DETAILS

Stimuli

Twenty-four fruits and vegetables were chosen as stimuli based on high familiarity (mean \pm SD = 6.13 \pm 0.35, obtained from a 7-point familiarity rating on an independent group of 59 college students). The names of these fruits and vegetables were all disyllabic words with the exception of the name of carrot being tri-syllabic. For the fMRI experiment, the names were digitally recorded (22050 Hz, 16 Bit), spoken by a female native Mandarin speaker. Stimulus presentation was controlled by E-prime (RRID:SCR_009567; [Schneider et al., 2002](#)).

Behavioral tests

then correlated the items in each group and thus obtained a 24×24 object RSM for each group. Object color spaces (Figure S1C) were further constructed by conducting MDS on these RSMs. Correlations between these object-color-generation-derived RSMs and RSMs obtained through direct object color similarity ratings were computed to investigate how well the object color space could be approximated by object-color verbal association.

We further approximated the object color space by combining object color name occurrences and the association between color names. We collected 7-point (1: most dissimilar, 7: most similar) pairwise color similarity ratings from both groups to measure the relationship among 9 color concepts (i.e., red, orange, yellow, green, cyan, blue, purple, pink, gold) (Figure S1B). To combine object color name occurrences with color name associations, we identified, from among the 9 frequent color words, the most frequently generated color for each fruit/vegetable item in the object color generation task as the representative color for that item. Then, the color similarity between fruit/vegetable items was defined as the similarity between the corresponding representative colors obtained from the color word similarity rating, resulting in a 24×24 object RSM for each group. Corresponding object color spaces (Figure S1D) were further constructed by conducting MDS on these RSMs. Note that the blind participant (B113) who was an outlier in the main experiment (pairwise similarity rating; see Figure S9) was also excluded here. Nevertheless, the above results pattern remained highly similar when this participant was not excluded.

Procedures for task-fMRI experiment

An object color verification fMRI experiment was performed to obtain object color representations in the sighted and blind participants, using spoken names of fruit and vegetables as stimuli. In addition, a color perceptual localizer experiment was conducted on a group of 14 sighted participants to functionally localize brain regions underlying color perception. Seven participants took part in both fMRI experiments.

Object color verification experiment

Participants listened to spoken names of 24 fruit and vegetable items and verified whether the item was red or not (Figure 2A). Participants pressed a button with their right index finger to give a “yes” response and pressed another button with right middle finger for a “no” response. There were three runs. Each run lasted 346 s, consisted of 72 3 s-long object trials (1 s auditory word followed by 2 s silence) and 36 3 s-long null-trials (3 s silence). Each object item was presented three times within each run. The order of the 108 trials was pseudorandomized, with the restriction that no two consecutive object trials were identical and the first and the last trials were object trials rather than null trials. Each run began with a 12 s silence period and ended with a 10 s silence period. Across the whole experiment, each of the 24 fruits and vegetables was presented 9 times. Independent pseudo-randomizations were created for each run in each participant.

Color perceptual localizer

The color perception localizer was an fMRI-adapted version of the Farnsworth-Munsell 100 Hue Task, which has been used previously to identify brain regions involved in color perception (Beauchamp et al., 1999; Simmons et al., 2007). During the experiment, participants saw blocks of 7 colored or grayscale wheels (Figure 3A) and judged whether the five wedges making up the wheel were uniformly ordered from lightest to darkest hue. Participants were asked to press a button with their right index finger if they found that the hues in the wheel were uniformly sequenced or otherwise press another button with the right middle finger. There were 4 runs in the color perception localizer. Each run lasted 230 s, consisted of 3 color wheel blocks and 3 grayscale wheel blocks, with all 6 blocks separated by 15 s-long fixation periods. Each block lasted 21 s, consisted of seven 2.5 s-long wheels separated by a 0.5 s black inter-stimulus interval. The block order was counterbalanced across runs. Each run began with a 12 s-long fixation period and ended with a 17 s-long fixation period.

Image acquisition

All functional and structural MRI data were collected using a Siemens Prisma 3T Scanner with 20-channel head-neck coil at the Center for MRI Research, Peking University.

The functional data were acquired with a simultaneous multi-slices (SMS) echoplanar imaging sequence supplied by Siemens (slice planes scanned along the rectal gyrus, 64 axial slices, phase encoding direction from posterior to anterior, repetition time (TR) = 2000 ms, echo time (TE) = 30 ms, multi-band factor = 2, flip angle (FA) = 90° , field of view (FOV) = 224 mm \times 224 mm, matrix size = 112 \times 112, slice thickness = 2 mm, gap = 0.2 mm, voxel size = 2 \times 2 \times 2.2 mm). The resting-state scanning lasted 8 minutes (240 volumes), during which the participants were asked to close their eyes and to not fall asleep. In addition, a high-resolution 3D T1-weighted anatomical scan was acquired using the magnetization-prepared rapid acquisition gradient echo (MPRAGE) sequence for anatomical reference (192 sagittal slices, TR = 2530 ms, TE = 2.98 ms, FA = 7° , FOV = 224 mm \times 256 mm, matrix size = 224 \times 256, interpolated to 448 \times 512, slice thickness = 1 mm, voxel size = 0.5 \times 0.5 \times 1 mm).

QUANTIFICATION AND STATISTICAL ANALYSIS

Data preprocessing

Task-fMRI data were preprocessed using Statistical Parametric Mapping software (SPM12; RRID:SCR_007037; <https://www.fil.ion.ucl.ac.uk/spm12/>) in the MATLAB (Mathworks; RRID: SCR_001622). For each individual participant in each experiment, the volumes ($n = 6$) of the silence/fixation block at the very beginning of each functional run were discarded for signal equilibrium.

Task-fMRI data first underwent slice timing correction. Then the images from multiple runs were aligned to the individual's first image of the first run using six rigid body transforming parameters. For multi-variate analyses, the realigned images were not further normalized or spatially-smoothed and the structural images were co-registered to the mean functional image. The deformation fields for the transformations between the Montreal Neurological Institute (MNI) space and the native space were obtained through segmentation. For univariate analyses, the realigned images were further normalized into the MNI space using unified segmentation and spatially smoothed using a 6mm full-width half-maximum (FWHM) Gaussian kernel.

Resting-state fMRI data were preprocessed using SPM12 and the toolbox for Data Processing & Analysis for Brain Imaging (DPABI, v3.1, RRID:SCR_010501, <http://fmri.org/DPABI>) (Yan et al., 2016) and analyzed using the Resting-State fMRI Data Analysis Toolkit V1.8 (RRID:SCR_009641; Song et al., 2011). For each participant, preprocessing follows conventional procedures, which include: 1) discarding the first 10 volumes for signal equilibrium; 2) slice timing; 3) correction for head movement with rigid body translation and rotation parameters; 4) normalization into MNI space by DARTEL (Ashburner, 2007); 5) spatial smoothing with 4mm FWHM Gaussian kernel; 6) removing the signal trend with time linearly; 7) band-pass (0.01-0.1Hz) filtering; 8) regressing out nuisance variables including the six rigid head motion parameters, the global signal averaged across the whole brain, the white matter signal averaged from the deep cerebral white matter and the cerebrospinal fluid signal averaged from the ventricles to further reduce non-neuronal signal confounds. Note that one blind participant was excluded from the subsequent resting-state functional connectivity analysis due to excessive head motion ($> 2\text{mm}/2^\circ$).

Data analysis

For each participant, general linear models (GLM) were built to obtain condition-specific beta estimates for subsequent analyses. For the event-related designed object color verification experiment, the unsmoothed, un-normalized data were analyzed using the GLM. The GLM for each run contains 24 regressors corresponding to the 24 fruit and vegetable names. For the block design color perceptual localizer, the smoothed, normalized data were analyzed. The GLM for each run contains two regressors corresponding respectively to the chromatic and achromatic conditions. For both experiments, no participant had head motion larger than $1.5\text{mm}/1.5^\circ$. Six head motion parameters were further included in each GLM as regressors of no interests to control for potential confounding of head motion. Each regressor was convolved with a canonical HRF and a high-pass filter cut-off was set as 128 s for the GLM of each run.

To investigate the object color representation in the brain of EB and SC participants, we conducted Representational Similarity Analyses (RSA) (Kriegeskorte et al., 2008) using a searchlight procedure (Kriegeskorte et al., 2006) in each individual participant. The t-value (each condition relative to baseline) images of the 24 fruit and vegetable names in the object color verification experiment were calculated to capture the activation patterns. The t-images were chosen to suppress the contribution of voxels with high beta estimates due to high noise (Misaki et al., 2010). For each participant, the structural image was co-registered to the mean functional image and segmented into different tissues. The resulting gray matter probabilistic image was resliced to the same spatial resolution as that of the functional image and thresholded at one-third to generate a binary mask for RSA searchlight mapping. For each voxel within the gray matter mask, the multi-condition activation patterns within a sphere (radius = 6mm) centered at that voxel were extracted to calculate the neural representational similarity matrix (RSM) based on that search sphere. Pearson correlations were computed between conditions and a 24×24 neural RSM was obtained for each search sphere and then compared with behavior-derived object color RSM using Spearman's rank correlation, or using partial Spearman's rank correlations to control for effects of other object features. The resulting correlation maps were Fisher transformed, normalized to the MNI space and spatially smoothed using a 6mm FWHM Gaussian kernel for subsequent group-level statistical analyses.

To test for significant object color representation in both groups, the correlation maps of all EB and SC participants were entered together into a group-level random-effects one-sample t test analysis using the permutation-based statistical nonparametric method mapping (SnPM; RRID:SCR_002092; <https://go.warwick.ac.uk/tenichols/snpm>). SnPM-based one-sample t test analysis was also conducted for each group respectively. The differences between EB and SC groups were investigated using SnPM-based two-sample t test analysis. No variance smoothing was used and 10000 permutations were performed.

Group-level random effects analyses were first conducted in anatomically pre-defined left anterior temporal lobe and inferior frontal cortex and in functionally defined color-sensitive ventral occipitotemporal cortical (VOTC) regions, respectively. These two regions were given special attention because they have been proposed as candidate brain substrates for representation of abstract concepts or functional/encyclopaedic knowledge with little or no sensory reference (Noppeney and Price, 2004; Striem-Amit et al., 2018; Wang et al., 2010) and for sensory-based object color representations, respectively (Bannert and Bartels, 2013, 2018; Goldberg et al., 2006; Hsu et al., 2011; Martin, 2016; Simmons et al., 2007). The left anterior temporal lobe and inferior frontal cortex mask (L-ATL/IFC; Figure 2B) was defined as the union of six anterior temporal regions and the inferior frontal cortex regions in the left hemisphere according to the Harvard-Oxford Atlas (probability > 0.2). These regions included the temporal pole (8#), the anterior superior temporal gyrus (9#), the anterior middle temporal gyrus (11#), the anterior inferior temporal gyrus (14#), the anterior temporal fusiform cortex (37#), the anterior parahippocampal gyrus (34#), the pars triangularis and the pars opercularis of the inferior frontal gyrus (5#, 6#), resulting in 5692 voxels (45536mm^3). The color-sensitive VOTC (VOTC-color; Figure 3A) was defined as regions showing stronger activation to chromatic stimuli relative to gray-scale stimuli (voxel-level $p < 0.001$, one-tailed, cluster-level FWE corrected $p < 0.05$) within the cerebral mask combining the posterior and temporooccipital divisions of inferior temporal gyrus (15#, 16#), the posterior divisions of parahippocampal gyrus (35#), the lingual gyrus (36#), the posterior division of temporal fusiform cortex (38#), the

temporal occipital fusiform cortex (39#) and the occipital fusiform gyrus (40#) in the Harvard-Oxford Atlas (probability > 0.2), resulting in 2664 voxels (21,312 mm³). Note that for the ROI-based rsFC analyses, a more stringent threshold (voxel level FWE corrected $p < 0.05$ across voxels in the below-described gray matter mask) was adopted to identify the seed ROI for the color perceptual system. The seed ROI for the language system was defined from a group-level language localizer which contrast sentences with nonword lists in 220 participants (Fedorenko et al., 2010; <https://evlab.mit.edu/funcloc/download-parcels>), including regions in the left hemisphere covering the lateral temporal regions, temporoparietal junction, inferior frontal gyrus and precentral gyrus. Group-level analyses were further conducted in a gray matter mask to explore object color representation in the whole brain. The gray matter mask was defined as voxels with a probability higher than one-third in the SPM12 gray matter template and within the cerebral regions (1#-90#) in the Automated Anatomical Labeling (AAL) template (Tzourio-Mazoyer et al., 2002), resulting in 111,493 voxels (891,944 mm³).

For the regions detected from the RSA searchlight mapping, we conducted regions of interest (ROI) analyses to further corroborate our findings. For each ROI, the voxel-wise Fisher-transformed correlation values obtained from RSA searchlight were extracted and averaged across all voxels within the ROI for each participant. Nonparametric bootstrap resampling t tests (Efron and Tibshirani, 1993) implanted in the SPSS software were conducted to compare the correlation values (number of bootstrap samples = 10000). In addition, to measure the strength of data in accepting or rejecting the null hypothesis, Bayesian t tests implanted in the JASP software (RRID:SCR_015823; version 0.9.2; <https://jasp-stats.org/>) were further conducted on the correlation values, with a default Cauchy prior width of $r = 0.707$ for effect size on the alternative hypothesis (H1) (Rouder et al., 2012). For the ROIs identified as showing significant object color representation from the combined-group one-sample t test, bootstrap resampling and Bayesian independent samples t test were conducted to test whether there was significant difference between the two groups (H1: EB \neq SC). For the ROIs identified as significant in one group, bootstrap resampling and Bayesian one-sample t tests were conducted to test whether the object color representation was significant in the other group (H1: group mean > 0). The brain results were projected onto the MNI brain surface using the BrainNet Viewer (RRID:SCR_009446; Xia et al., 2013) (<https://www.nitrc.org/projects/bnv>).